Theoretical study of the optical gain characteristics of a $Ge_{1-x}Sn_x$ alloy for a short-wave infrared laser*

Zhang Dong-Liang(张东亮), Cheng Bu-Wen(成步文)†, Xue Chun-Lai(薛春来), Zhang Xu(张 旭), Cong Hui(丛 慧), Liu Zhi(刘 智), Zhang Guang-Ze(张广泽), and Wang Qi-Ming(王启明)

State Key Laboratory on Integrated Optoelectronics, Institute of Semiconductors, Chinese Academy of Sciences, Beijing 100083, *China*

(Received 13 July 2014; revised manuscript received 4 September 2014; published online 10 December 2014)

Optical gain characteristics of $Ge_{1-x}Sn_x$ are simulated systematically. With an injection carrier concentration of 5×10^{18}/cm^3 at room temperature, the maximal optical gain of $Ge_{0.922}Sn_{0.078}$ alloy (with n-type doping concentration being 5×10^{18}/cm^3) reaches 500 cm^{-1}. Moreover, considering the free-carrier absorption effect, we find that there is an optimal injection carrier density to achieve a maximal net optical gain. A double heterostructure $Ge_{0.554}Si_{0.289}Sn_{0.157}$/$Ge_{0.922}Sn_{0.078}$/$Ge_{0.554}Si_{0.289}Sn_{0.157}$ short-wave infrared laser diode is designed to achieve a high injection efficiency and low threshold current density. The simulation values of the device threshold current density J_{th} are 6.47 kA/cm^2 (temperature: 200 K, and $\lambda = 2050$ nm), 10.75 kA/cm^2 (temperature: 200 K, and $\lambda = 2000$ nm), and 23.12 kA/cm^2 (temperature: 300 K, and $\lambda = 2100$ nm), respectively. The results indicate the possibility to obtain a Si-based short-wave infrared $Ge_{1-x}Sn_x$ laser.

Keywords: infrared, GeSn alloys, semiconductor lasers, optoelectronic

PACS: 42.55.Px, 42.70.Hj, 78.40.Fy, 95.85.Jq **DOI:** 10.1088/1674-1056/24/2/024211

1. Introduction

Silicon photonics have diverse applications in optoelectronic integration, high-speed optical communications, and ultrafast signal processing. The key Si photonic components, including modulators, photodetectors, waveguides, filters, etc., have been demonstrated.[1] But the indirect band-gap of group IV semiconductor challenges the realization of laser sources because of the very low probability of indirect radiative recombination. However, germanium has a slight energy difference (136 meV) between the direct band-gap and the indirect band-gap, which increases the probability of radiative recombination between the Γ valley and the valence band. It has been indicated that heavy n-type doping and tensile strain engineering can effectively provide population inversion in the direct band Γ valley of Ge, and a net gain of 400/cm can be obtained theoretically.[2] Using this method, researchers have recently realized optically pumping[3] and electrically pumping[4] Ge lasers. However, the electrically pumping Ge laser needs heavy n-type doping and a high threshold current density (about 218 kA/cm^2), which induces the intensive free-carrier absorption (FCA) and instantaneous breakdown of the metal contact. Such extreme conditions greatly hinder its practical applications. Adequate tensile-strain to reduce the energy difference between Γ valley and L valley plays a pivotal role in reducing the threshold current. However, it is very difficult to achieve high tensile-strain in Ge while keeping its high crystal quality and sufficient thickness.

Fortunately, the introduction of Sn into Ge is expected to diminish the direct band-gap to a larger extent than the indirect band-gap. High quality $Ge_{1-x}Sn_x$ alloy epitaxy by MBE was reported from our previous work.[5] Recently, $Ge_{1-x}Sn_x$ p–i–n photodetectors for detecting all telecommunication bands ($x = 3\%$)[6] and short-wave infrared ($x = 3.64\%$)[7] have been reported. Moreover, many experiments and theories have indicated that a $Ge_{1-x}Sn_x$ alloy with a Sn percentage of about 6%-10% is a kind of prospective direct band-gap material.[8–11] Several experiments have successfully been conducted to study the photoluminescences of $Ge_{1-x}Sn_x$ materials. Mid-infrared electroluminescence from GeSn/Ge heterojunction on a Si substrate has also been reported.[12,13] In Ref. [14], an electrically injected p–i–n SiGeSn/$Ge_{0.922}Sn_{0.078}$/SiGeSn double heterostructure (DHS) diode was designed and it was estimated that $Ge_{1-x}Sn_x$ becomes a pseudo-direct band semiconductor when the Sn composition was about 6%, while the bowing parameter about direct band-gap used in the paper does not accord with the latest experimental result.[11] In addition, the key factor of the FCA effect was not considered.

In the present paper, the optical gain characteristics of direct band $Ge_{1-x}Sn_x$ alloys are systematically investigated. The effects of the L indirect band valley, the temperature, the injected current density, the proportions of Sn, the Auger process, and the free-carrier absorption effect are taken into consideration in our calculations. A double heterostructure $Ge_{0.554}Si_{0.289}Sn_{0.157}$/$Ge_{0.922}Sn_{0.078}$/$Ge_{0.554}Si_{0.289}Sn_{0.157}$ short-wave infrared laser diode is then designed to achieve

*Project supported by the Major State Basic Research Development Program of China (Grant No. 2013CB632103), the National High-Technology Research and Development Program of China (Grant No. 2012AA012202), and the National Natural Science Foundation of China (Grant Nos. 61177038 and 61176013).

†Corresponding author. E-mail: cbw@red.semi.ac.cn

© 2015 Chinese Physical Society and IOP Publishing Ltd

high injection efficiency and low threshold current density. Finally, the device threshold current densities are simulated at different temperatures and wavelengths.

2. Theoretical model description and simulation results

The physical parameters of $Ge_{1-x}Sn_x$ or $Si_xGe_{1-x-y}Sn_y$ can be obtained using the linear interpolation formulae, excluding the band-gap. There is a nonlinear relationship between alloy band-gap $E_g^{alloy}(x)$ and the alloy composition x. As far as $Ge_{1-x}Sn_x$ alloys are concerned, the band-gap is usually calculated by a parabolic function, which is listed as follows:

$$\begin{aligned} E_g^{GeSn}(x) &= (1-x)\times E_{gGe} + x\times E_{gSn} - b_{GeSn}x(1-x), \quad (1)\\ E_g^{SiGeSn}(x,y) &= (1-x-y)\cdot E_{gGe} + x\cdot E_{gSn}\\ &\quad + y\cdot E_{gSi} - b_{GeSn}x(1-x-y)\\ &\quad - b_{GeSi}y(1-x-y) - b_{SiSn}xy, \quad (2) \end{aligned}$$

where x is the Sn percentage, y is the Si percentage, and b is bowing parameter.

For a $Ge_{1-x}Sn_x$ alloy, $b_L = 0.89$[8] and $b_\Gamma = 2.1$[11] are cited from the latest result; for GeSi and SiSn, $b_\Gamma = 0.21$ and 13.2,[15] respectively. Figure 1(a) shows the direct band-gap $E_{g,\Gamma}$ and indirect band-gap $E_{g,L}$ of $Ge_{1-x}Sn_x$ alloy, each as a function of Sn percentage at room temperature. The band parameters of Si, Ge, and Sn are cited from the data handbook.[16] In order to obtain a more precise result the temperature-dependence of the Ge band-gap is taken into account (that of Sn is neglected because of its low percentage), as follows:[17]

$$\begin{aligned} E_{gL} &= 0.742 - \frac{4.8\times10^{-4}\times T^2}{T+235},\\ E_{g\Gamma} &= 0.89 - \frac{5.82\times10^{-4}\times T^2}{T+296} \quad (E_g \text{ in eV, and } T \text{ in K}). \quad (3) \end{aligned}$$

As figure 1(a) shows, when x (Sn) equals 7.8%, the direct and indirect band-gap reach the same value (about 0.56 eV). Based on this model, the band parameters of $Ge_{1-x}Sn_x$ alloys, with x in a range between 0% and 15% (0%, 3%, 6%, 7.8%, 10%, 12%, and 15% are chosen in the calculation) are calculated and then utilized for the next optical simulations.

The E–k relation between electron and hole are assumed to be parabolic, as follows:

$$\begin{aligned} E_e &= E_{c\Gamma,L} + \frac{\hbar^2k^2}{2m_{c\Gamma,L}} \quad \text{for electrons},\\ E_h &= E_v - \frac{\hbar^2k^2}{2m_{hh,lh}} \quad \text{for holes}. \quad (4) \end{aligned}$$

And the photon energy $h\nu$ emitting through Γ–h transition is given as follows:

$$\begin{aligned} h\nu &= E_e - E_h = (E_{c\Gamma} - E_v) + \frac{\hbar^2k^2}{2}\left(\frac{1}{m_{c\Gamma}} + \frac{1}{m_{hh,lh}}\right)\\ &= E_g + \frac{\hbar^2k^2}{2m_r} \quad \text{and} \quad m_r = \frac{m_{c\Gamma}m_{hh,lh}}{m_{c\Gamma}+m_{hh,lh}}. \quad (5) \end{aligned}$$

According to Eq. (5), the electron energy in the Γ valley E_e and hole energy E_h are described by

$$\begin{aligned} E_e &= E_{c\Gamma} + \frac{m_r}{m_{c\Gamma}}(h\nu - E_g),\\ E_h &= E_v - \frac{m_r}{m_{hh,lh}}(h\nu - E_g). \quad (6) \end{aligned}$$

In a steady state, electrons and holes obey quasi-Fermi distribution, which is described by electron quasi-Fermi level E_{fc} and hole quasi-Fermi level E_{fv}. When the energy difference between an electron (E_e) and a hole (E_h) with the same k in the reciprocal space is equal to photon energy $E = h\nu$, the occupation probabilities of an electron and a heavy hole are described, respectively, by

$$\begin{aligned} f_c &= \left(1+\exp\left(\frac{E_e - E_{fc}}{k_BT}\right)\right)^{-1},\\ f_v &= \left(1+\exp\left(\frac{E_{fv} - E_h}{k_BT}\right)\right)^{-1}. \quad (7) \end{aligned}$$

Quasi-Fermi level values (E_{fc} and E_{fv}) corresponding to injected carrier density $N_{inj} = P_{inj}$ and doping density N_D under a degenerate condition (with heavy doping and high injection) can be obtained by the calculation method from the second chapter of Ref. [18] through the following relationship:

$$n_L + n_\Gamma = N_{inj} + N_D^+, \quad p_{lh} + p_{hh} = P_{inj}. \quad (8)$$

The percentage of electrons occupying Γ band valley can then be obtained as

$$\eta = \frac{n_\Gamma}{n_L + n_\Gamma}. \quad (9)$$

Compared with the direct Γ band valley, the indirect L band valley of Ge or $Ge_{1-x}Sn_x$ can accommodate a majority of electrons because of its lower energy valley, high degeneracy ($s = 4$), and the bigger effective mass of the electron. Even worse, the electron in the indirect L band valley has a very low emission transition probability and high contribution of free-carrier absorption. While the key point for the laser process is to achieve considerable stimulated radiation from a direct Γ valley, the indirect L band valley has a serious negative influence on this material luminescence quantum efficiency.

Figure 1(b) shows the percentage of electrons occupying the Γ band valley of $Ge_{1-x}Sn_x$ with x value being between 0% and 15% (n-doping density: $1\times10^{18}/cm^3$, injected carrier density is 1×10^{19} cm^{-3}; room temperature: 300 K). It is indicated that the percentage of electrons occupying the Γ band valley of $Ge_{0.88}Sn_{0.12}$ is 1000 times as high as that of Ge; however, that of pseudo-direct band $Ge_{0.922}Sn_{0.078}$ alloy is still only about 1%, as shown in Fig. 1(b).

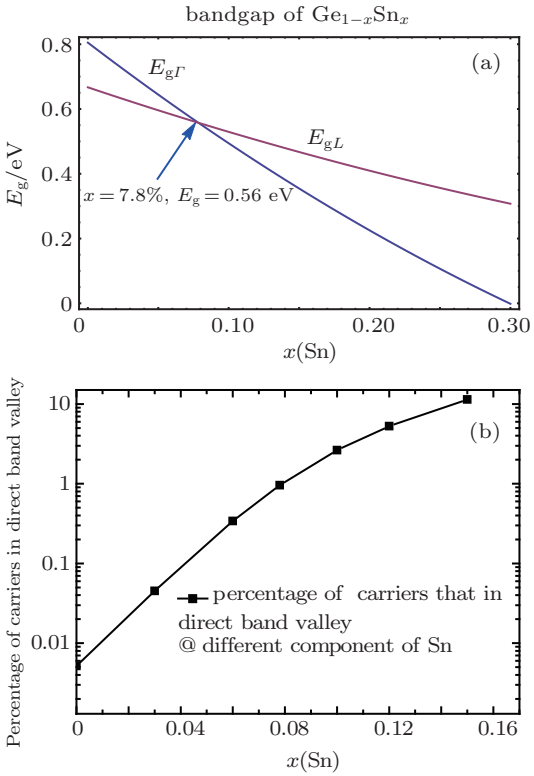


Fig. 1. (color online) (a) The L and Γ conduction band band-gaps of $Ge_{1-x}Sn_x$ alloy each as a function of Sn percentage at room temperature. (b) The variation of the percentage of electrons in Γ conduction valley of $Ge_{1-x}Sn_x$ with x in a range between 0% and 15% at room temperature.

After the calculation of band structure and carrier distribution, the optical gain spectrum ($g_{\Gamma-\mathrm{hh}}$) and the spontaneous emission spectrum ($R_{\mathrm{sp}\Gamma-\mathrm{hh}}$) through Γ–hh radiative recombination can be obtained; the formulae are given as follows:[19]

$$g_{\Gamma-\mathrm{hh}} = \left(\frac{ehM_\mathrm{b}^2}{4\pi^2\varepsilon_0 m_0^2 c n_0 h\nu}\right)\left(\frac{2m_\mathrm{r}m_0}{\hbar^2}\right)^{1.5} \times\sqrt{h\nu - E_\mathrm{g}}(fc(E_\mathrm{e})+f_\mathrm{v}(E_\mathrm{h})-1), \quad (10)$$

$$R_{\mathrm{sp}\Gamma-\mathrm{hh}}(h\nu) = \frac{n_0\times e^2\times M_\mathrm{b}^2\times h\nu}{\pi m_0^2\varepsilon_0 h^2 c^3}\left(\frac{2}{\hbar^2}\frac{m_{\mathrm{c}\Gamma}\times m_\mathrm{hh}}{m_\mathrm{hh}+m_{\mathrm{c}\Gamma}}\right)^{1.5} \times\sqrt{h\nu - E_\mathrm{g}}f_c(E_\mathrm{e})\times f_\mathrm{v}(E_\mathrm{h}), \quad (11)$$

where e is the electron charge, m_0 is the free electron mass, ε_0 is the permittivity of vacuum, h is the Planck constant ($\hbar = h/2\pi$), c is the speed of light in vacuum, n_0 is the index of refraction, $m_{\mathrm{c}\Gamma}$ is the effective mass of electron in Γ band valley, m_hh is the heavy hole mass, m_lh is the light hole mass, E_g is the band gap, and M_b^2 is the average matrix element for the Bloch states.

The optical gain spectrum $g_{\Gamma-\mathrm{lh}}$ and the spontaneous emission spectrum $R_{\mathrm{sp}\Gamma-\mathrm{lh}}$ through Γ–lh radiative recombination can be obtained in a similar way, i.e., just replacing m_hh in Eqs. (10) and (11) with m_lh. Thus, the total optical gain spectrum $G(h\nu)$ and the spontaneous emission rate R_sp are given as follows:

$$G(h\nu) = g_{\Gamma-\mathrm{lh}}(h\nu) + g_{\Gamma-\mathrm{hh}}(h\nu)$$

$$R_\mathrm{sp} = \int_{E\mathrm{g}}^{\infty}(R_{\mathrm{sp}\Gamma-\mathrm{hh}}+R_{\mathrm{sp}\Gamma-\mathrm{lh}})\,\mathrm{d}(h\nu). \quad (12)$$

The total optical gain spectra of $Ge_{1-x}Sn_x$ with different Sn percentages and with a same injected carrier density (5×10^{18}/cm^3) and doping density (5×10^{18}/cm^3) at room temperature are then calculated and shown in Fig. 2(a). The optical gain significantly increases with the increase of Sn percentage. The maximal gain coefficient of $Ge_{1-x}Sn_x$ alloy increases from 200/cm ($x = 7.8\%$) to 1000/cm ($x = 15\%$), which indicates that the introduction of Sn into Ge can promote optical gain evidently and may reduce threshold carrier density. The decrease of threshold carrier density also reduces the FCA and Auger recombination process, which will further lower the threshold current density.

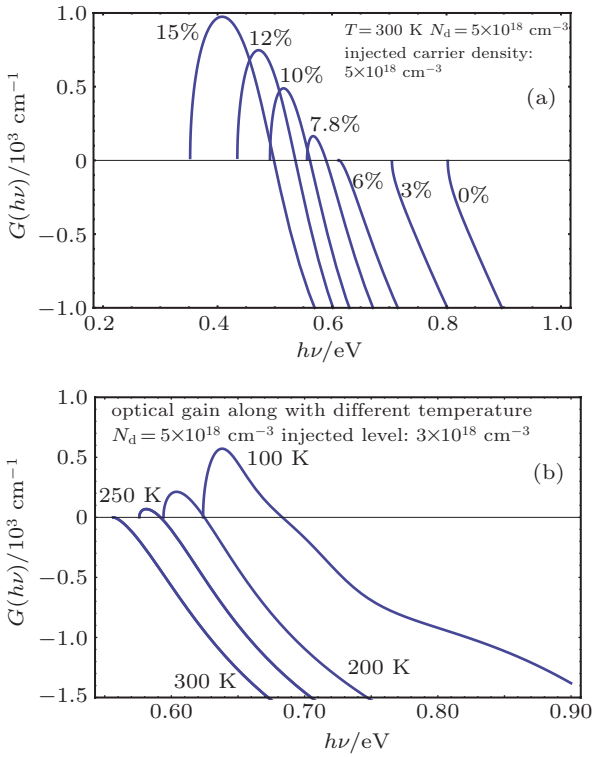


Fig. 2. (color online) (a) Total optical gains of $Ge_{1-x}Sn_x$ ($x = 0$, 3, 6, 7.8, 10, 12, 15% respectively) with a same injected carrier density (5×10^{18}/cm^3) and doping level (5×10^{18}/cm^3) at room temperature. (b) Optical gain spectra of alloy with 7.8% Sn at different temperatures.

Optical gain spectra of alloy with 7.8% Sn (injected carrier density: 5×10^{18}/cm^3, n-doping level: 3×10^{18}/cm^3) at different temperatures are simulated. As figure 2(b) indicates, it is hard for $Ge_{0.922}Sn_{0.078}$ to realize optical amplification at 300 K under this carrier density condition, but a low temperature can improve optical gain effectively and the maximal gain can reach 500 cm^{-1} at 100 K. The blue shift of maximal gain is due to the band-gap broadening at low temperatures.

The optical gain spectra of a $Ge_{0.922}Sn_{0.078}$ alloy with four different injected carrier densities are also studied (n-doping concentration: 5×10^{18}/cm^3, and temperature: 300 K), as shown in Fig. 3(a). Although $Ge_{0.922}Sn_{0.078}$ has become a direct band-gap semiconductor, a high injection density, such

as 6×10^{18}/cm^3, is needed to achieve population inversion in direct Γ band valley and provide significant positive optical gain. In addition, a comparison between $Ge_{0.922}Sn_{0.078}$ and Ge with an identical injected carrier density of 9×10^{18}/cm^3 is made. It is indicated by the dashed line and solid line in Fig. 3(a) that the maximum gain of $Ge_{0.922}Sn_{0.078}$ can reach 500 cm^{-1}, while the optical gain of Ge is still negative.

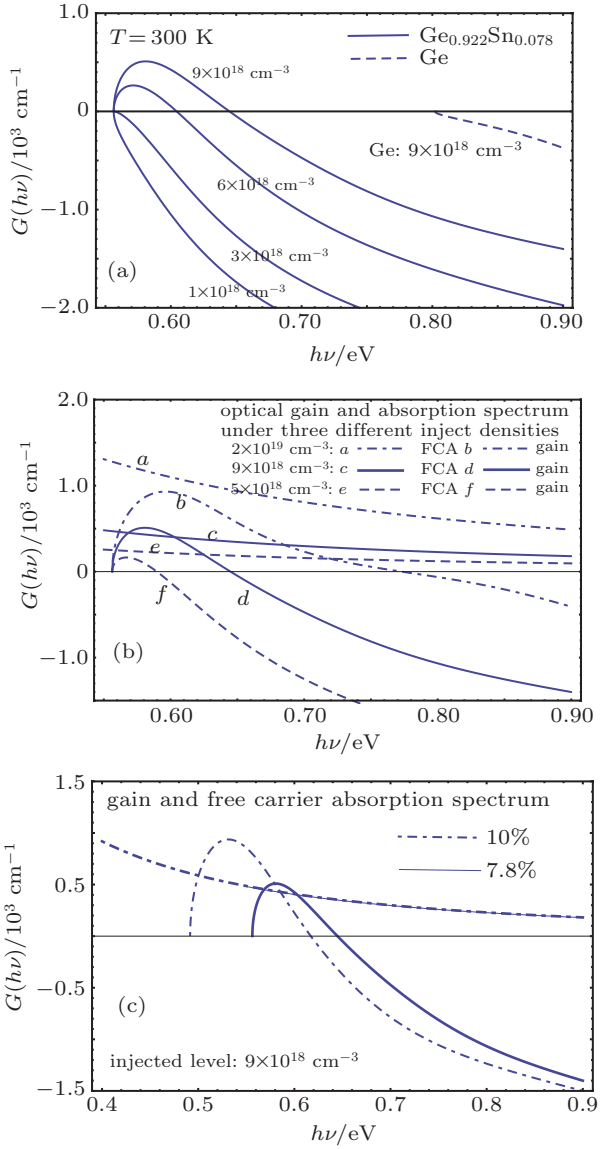


Fig. 3. (color online) (a) Optical gain spectra of $Ge_{0.922}Sn_{0.078}$ alloy with four different injected carrier densities and a comparison with Ge. (b) The optical gain and FCA spectra of $Ge_{0.922}Sn_{0.078}$ alloy simulated with the injected carrier densities of 5×10^{18}, 9×10^{18}, 2×10^{19} cm^{-3}, respectively. (c) Comparison between optical gain and FCA of $Ge_{0.922}Sn_{0.078}$ alloy and that of $Ge_{0.9}Sn_{0.1}$ on an identical injection and n-doping level at room temperature.

It is obvious that high injection could contribute to the achievement of high optical gain; however, the FCA effect is considerable in high doping or at a high injection level, which is bad for optical gain. The FCA effect, consisting of the absorptions of L-conduction valleys, Γ-conduction valley, heavy-hole band, and light-hole band, can be described by Drude–Lorentz equation[20] as follows:

$$\alpha_{\mathrm{FCA}} = \frac{e^3\lambda^2}{4\pi^2c^3\varepsilon_0 n_0}\left(\frac{n_\Gamma}{\mu_\Gamma\times m_{c\Gamma}^2}+\frac{n_L}{\mu_L\times m_{cL}^2}+\frac{p_{\mathrm{hh}}}{\mu_{\mathrm{P}}\times m_{\mathrm{hh}}^2}+\frac{p_{\mathrm{lh}}}{\mu_{\mathrm{P}}\times m_{\mathrm{lh}}^2}\right), \tag{13}$$

where λ is the free space wavelength; n_Γ and n_L are the electron densities in the Γ- and L-conduction valleys, respectively; p_{hh} and p_{lh} are the hole densities in the heavy and light valence band, respectively; $m_{c\Gamma}$ and m_{cL} are the electron effective mass values of the Γ- and L-conduction valleys, respectively; m_{hh} and m_{lh} are the heavy and light hole effective masses; μ_L and μ_Γ are the electron mobilities in the L- and Γ-conduction valleys, respectively; and, μ_{P} is the hole mobility in the valence band.

Moreover, the $Ge_{1-x}Sn_x$ carrier mobility (μ_L, μ_Γ, and μ_{P}) dependences of temperature and carrier density could be estimated by that of Ge for simplicity. The motilities in undoped Ge at the values of temperature T (100 K–300 K) are given by[16]

$$\mu_L(T) = \frac{4.9\times10^7}{T^{1.66}}\mathrm{cm}^2\cdot\mathrm{V}^{-1}\cdot\mathrm{s}^{-1}\quad(T\text{ in }K),$$
$$\mu_{\mathrm{p0}}(T) = \frac{1.05\times10^9}{T^{2.33}}\mathrm{cm}^2\cdot\mathrm{V}^{-1}\cdot\mathrm{s}^{-1}\quad(T\text{ in }K). \tag{14}$$

In addition, the mobility is also carrier-concentration-dependent, and the electron mobility of L-conduction valley and hole mobility of Ge (electron density of L-conduction valley: n_{L}, and hole density: n_{p}) at 300 K is given by[21,22]

$$\mu_L = \frac{\mu_{L0}(T)}{\sqrt{1+n_L\times10^{-17}}},$$
$$\mu_{\mathrm{p}} = \frac{\mu_{\mathrm{p0}}(T)}{\sqrt{1+n_{\mathrm{p}}\times2.1\times10^{-17}}},\quad(T=300\text{ K}). \tag{15}$$

The above equations are extended to other temperatures reasonably, and equation (14) is substituted into Eq. (15) to obtain $\mu_L(n,T)$ and $\mu_{\mathrm{p}}(p,T)$ each as a function of carrier density n and p (in cm^{-3}) at T (in K). However, to date there are no experimental data about the mobility of electrons the in Ge Γ-conduction valley. The relationship like Eq. (16) and Eq. (17) is then assumed to be

$$\mu_\Gamma = \frac{\mu_{\Gamma0}(T)}{\sqrt{1+n_\Gamma\times10^{-17}}}, \tag{16}$$
$$\frac{\mu_{L0}(T)}{\mu_{\Gamma0}(T)} = \frac{m_L}{m_\Gamma}. \tag{17}$$

Finally, the FCA spectra of $Ge_{1-x}Sn_x$ alloys as a function of carrier density and temperature can be obtained through Eqs. (13)–(17). For the optimization of injection density, the optical gain and FCA spectra of the $Ge_{0.922}Sn_{0.078}$ alloy

are simulated simultaneously with injected carrier densities of 5×10^{18}, 9×10^{18}, and 2×10^{19} cm^{-3}, respectively. The net gain is defined to simplify the description as follows:

$$g_{\rm net}(h\nu) = {\rm G}(h\nu) - \alpha_{\rm FCA}(h\nu). \quad (18)$$

As shown by the three curves b, d, f in Fig. 3(b), $\alpha_{\rm FCA}$ is inversely proportional to $(h\nu)^2$ and increases with the increase of carrier density. Moreover, $g_{\rm net}(h\nu)$ is negative for the photon energy between 0.55 eV and 0.90 eV when the injected carrier density is 5×10^{18} cm^{-3}, as shown by curve e and curve f in Fig. 3(b); when the density goes to 9×10^{18} cm^{-3}, $g_{\rm net}(h\nu)$ is positive within a certain value range of photon energy, as shown by curve c and curve d; when the injected carrier density reaches 2×10^{19} cm^{-3}, $g_{\rm net}(h\nu)$ is negative again, as shown by curve a and curve b. So it is concluded that the injected carrier density is not better higher, there should be an optimal injection to reach a maximal net gain for a special wavelength. In addition, as shown in Fig. 3(c), the comparisons of $G(h\nu)$ and $\alpha_{\rm FCA}$ between $Ge_{0.922}Sn_{0.078}$ and $Ge_{0.9}Sn_{0.1}$ with the same injection level indicate that the FCAs of both alloys almost coincide but the maximal optical gain value of $Ge_{0.9}Sn_{0.1}$ alloy is much higher than that of $Ge_{0.922}Sn_{0.078}$.

In a real device simulation, when the $G(h\nu)$ and $\alpha_{\rm FCA}(h\nu)$ of the active layer are obtained, the device threshold carrier density $n_{\rm th}$ can be obtain from the following equation at a given wavelength $(h\nu)$:

$$\Gamma \times G(n_{\rm th}) = \alpha_{\rm i}(n_{\rm th}) + \alpha_{\rm m}, \quad \alpha_{\rm m} = \frac{1}{2L}\ln\left(\frac{1}{R_1R_2}\right), \quad (19)$$

where Γ is the confinement factor, $\alpha_{\rm i}$ is the internal loss, mainly including FCA ($\alpha_{\rm i} \sim \alpha_{\rm FCA}$), $\alpha_{\rm m}$ is the mirror loss, L is the cavity length, R_1 and R_2 are the reflectivities of the front and back mirror, respectively. When the net optical gain

$${\rm G}_{\rm net}(h\nu) = \Gamma \cdot {\rm G}(h\nu) - \alpha_{\rm FCA}(h\nu) - \alpha_{\rm m} \quad (20)$$

is positive, which means that the optical gain can overcome the loss, the lasing can occur.

In this real device simulation, $Ge_{0.922}Sn_{0.078}$ is chosen as an active region because it is difficult to achieve the high Sn percentage alloy by the epitaxy technique.[23] In order to obtain high injection efficiency and low threshold current density, a double heterojunction (DHS) diode is designed. Figure 4(a) shows the band-gap and band-offset of $Ge_{1-x-y}Si_xSn_y$ cladding layer (lattice-matched to $Ge_{0.922}Sn_{0.078}$ active region), each as a function of Sn percentage y. For well confining the carriers and light, the cladding layer of $Ge_{0.554}Si_{0.289}Sn_{0.157}$ ($y = 0.157$) can have the largest band-gap difference with $Ge_{0.922}Sn_{0.078}$ layer: $\Delta E_{\rm g} = 215$ meV, valence-band-offset $\Delta E_{\rm v} = 95$ meV and conduction-band-offset $\Delta E_{\rm c} = 120$ meV. The DHS laser device as shown in Fig. 4(b) is designed. In the next device simulation, $\alpha_{\rm m}$ is assumed to be 10 cm^{-1} and Γ is assumed to be 1.

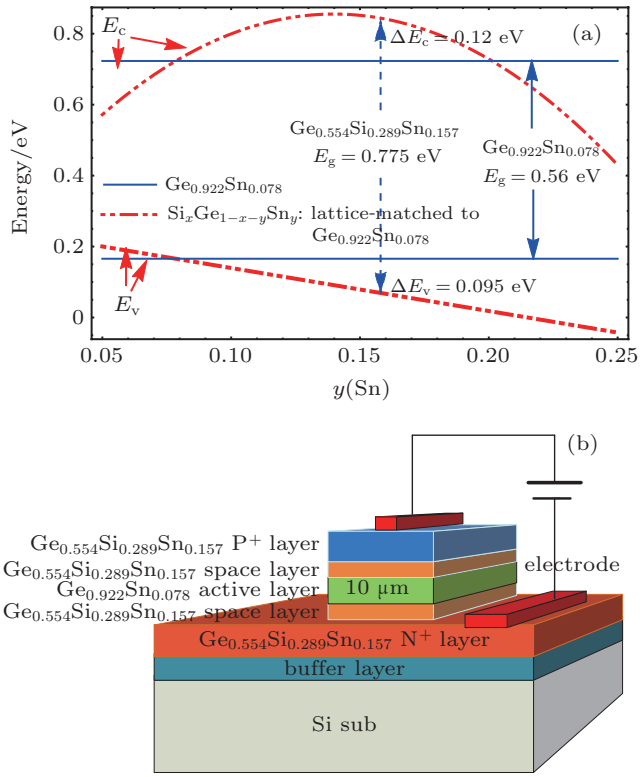


Fig. 4. (color online) (a) Band-gap and band offset of $Ge_{0.922}Sn_{0.078}$ active region and lattice-matched $Ge_{1-x-y}Si_xSn_y$ cladding layer each as a function of Sn percentage (y). (b) The designed Si-based double heterojunction laser device.

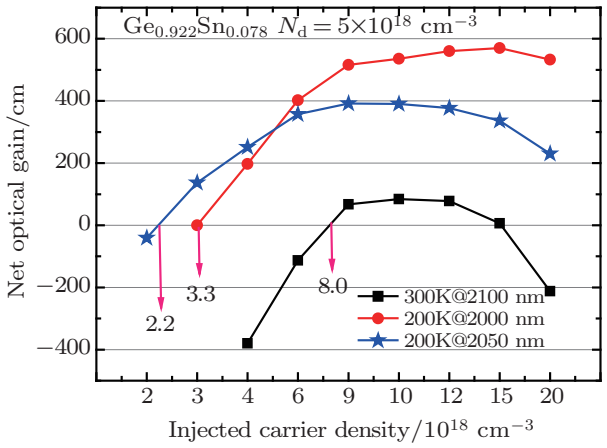


Fig. 5. (color online) Net gains versus injected carrier density (lasing wavelengths are 2000 nm and 2050 nm at 200 K, and 2100 nm at 300 K).

The $G_{\rm net}(h\nu)$ spectrum of $Ge_{0.922}Sn_{0.078}$ alloy (doping density: 5×10^{18} cm^{-3}) as a function of injection level is calculated at a given wavelength of λ, the threshold carrier density $n_{\rm th}$ can then be obtained where $G_{\rm net}(h\nu)$ equals zero. The net gain spectra of three different wavelengths,

each as a function of injected carrier density, are shown in Fig. 5, and the arrow-marked threshold carrier densities are about 8×10^{18} cm^{-3} (temperature: 300 K, and $\lambda = 2100$ nm), 2.2×10^{18} cm^{-3} (temperature: 200 K, and $\lambda = 2050$ nm), and 3.3×10^{18} cm^{-3} (temperature: 200 K, and $\lambda = 2000$ nm), respectively. $G_{\rm net}(h\nu)$ at room temperature is much smaller than at 200 K. In addition, the maximal values of $G_{\rm net}(h\nu)$ of these three conditions all appear at about $n \sim 9\times10^{18}$ cm^{-3}.

The the injected threshold current density $J_{\rm th}$ corresponding to threshold carrier density $n_{\rm th}$ can then be estimated according to the following formula:

$$\eta_{\rm i}\frac{J_{\rm th}}{ed} = R_{\rm sp}(n_{\rm th}) + R_{\rm Aug}(n_{\rm th}), \tag{21}$$

where $\eta_{\rm i}$ is the injection efficiency, and assumed to be 0.8; d is the depth of active region, and assumed to be 10 μm: $R_{\rm sp}$ is the spontaneous emission rate (as Eq. (12)), and $R_{\rm Aug}$ is the Auger recombination rate, which is neglected at 200 K when considering that the Auger recombination coefficient of $Ge_{0.922}Sn_{0.078}$ is small at low temperatures (there is no report at present). However, the $R_{\rm Aug}$ of $Ge_{0.922}Sn_{0.078}$ at room temperature is estimated through using Auger recombination coefficients of Ge, as shown in Eq. (22), which are $C_{\rm ppn} = 7.0\times10^{-32}$ cm^6/s[24] and $C_{\rm nnp} = 3.0\times10^{-32}$ cm^6/s.[25]

$$\begin{aligned} R_{\rm Aug-ccch}(n_{\rm th}) &= C_{\rm nnp}\times n_\Gamma^2\times p,\\ R_{\rm Aug-chhl}(n_{\rm th}) &= C_{\rm ppn}\times p^2\times n_\Gamma,\\ R_{\rm Aug} &= R_{\rm Aug-ccch}(n_{\rm th}) + R_{\rm Aug-chhl}(n_{\rm th}). \end{aligned} \tag{22}$$

The corresponding values of $J_{\rm th}$ are then obtained through Eqs. (12), (21), and (22), respectively, as 6.47 kA/cm^2 (temperature: 200 K, and $\lambda = 2050$ nm), 10.75 kA/cm^2 (temperature: 200 K, and $\lambda = 2000$ nm), and 23.12 kA/cm^2 (temperature: 300 K, and $\lambda = 2100$ nm). All of the above simulation results are shown in Table 1. These results indicate the possibility of obtaining a GeSn short-wave infrared laser at room temperature.

Table 1. Threshold carrier densities, spontaneous emission rates, Auger recombination rates, and threshold current densities at different temperatures and wavelengths.

Temperature/K	Wavelength/nm	$n_{\rm th}$/cm^{-3}	$R_{\rm sp}$/cm$^{-3}\cdot$s^{-1}	$R_{\rm Aug}$/cm$^{-3}\cdot$s^{-1}	$J_{\rm th}$/(kA/cm^{-2})
200	2000	3.3×10^{18}	5.37×10^{25}	neglected	10.75
200	2050	2.2×10^{18}	3.23×10^{25}	neglected	6.47
300	2100	8.0×10^{18}	1.14×10^{26}	1.12×10^{24}	23.12

3. Discussion and conclusion

In this paper the optical gain characteristics of $Ge_{1-x}Sn_x$ are systematically stimulated. $Ge_{1-x}Sn_x$ can become a direct band material when the Sn concentration is larger than 7.8%. Owing to the reduction of the energy difference between direct and indirect conduction band valley with the increase of Sn concentration, the percentage of the direct band electrons increases evidently, which contributes to the realization of population inversion in direct Γ band valley and significant optical gain. The maximal gain value of $Ge_{0.922}Sn_{0.078}$ reaches 500/cm, while that of Ge is still negative at room temperature (the doping carrier density and injected carrier density both are 5×10^{18} cm^{-3}). The simulation results indicate that there should be an optimal injection to reach a maximal net gain when the FCA effect is considered. To achieve a high injection efficiency and low threshold current density, a double heterojunction $Ge_{0.554}Si_{0.289}Sn_{0.157}/Ge_{0.922}Sn_{0.078}/Ge_{0.554}Si_{0.289}Sn_{0.157}$ short-wave infrared laser diode is designed and simulated. Through calculating the spontaneous emission rate and Auger recombination rate in $Ge_{0.922}Sn_{0.078}$, the injected threshold current densities $J_{\rm th}$ are obtained, which are about 6.47 kA/cm^2 (temperature: 200 K, and $\lambda = 2050$ nm), 10.75 kA/cm^2 (temperature: 200 K, and $\lambda = 2000$ nm), and 23.12 kA/cm^2 (temperature: 300 K, and $\lambda = 2100$ nm). They are of the same order of magnitude as III–V devices and indicate the possibility of obtaining a GeSn short-wave infrared laser at room temperature. Therefore, GeSn alloy is a promising candidate material, not only for all telecommunication bands in optoelectronics but also for shortwave infrared applications.

References

[1] Reed G T and Knights A P 2008 *Silicon Photonics* (Chichester; Hoboken, NJ: John Wiley & Sons)

[2] Liu J, Sun X, Pan D, Wang X, Kimerling L C, Koch T L and Michel J 2007 *Opt. Express* **15** 11272

[3] Liu J F, Sun X C, Kimerling L C and Michel J 2009 *Opt. Lett.* **34** 1738

[4] Camacho-Aguilera R E, Cai Y, Patel N, Bessette J T, Romagnoli M, Kimerling L C and Michel J 2012 *Opt. Express* **20** 11316

[5] Wang W, Su S J, Zheng J, Zhang G Z, Zuo Y H, Cheng B W and Wang Q M 2011 *Chin. Phys. B* **20** 068103

[6] Su S J, Cheng B W, Xue C L, Wang W, Cao Q A, Xue H Y, Hu W X, Zhang G Z, Zuo Y H and Wang Q M 2011 *Opt. Express* **19** 6408

[7] Zhang D L, Xue C L, Cheng B W, Su S J, Liu Z, Zhang X, Zhang G Z, Li C B and Wang Q M 2013 *Appl. Phys. Lett.* **102** 141111

[8] Yin W J, Gong X G and Wei S H 2008 *Phys. Rev. B* **78** 161203

[9] D'Costa V R, Fang Y Y, Tolle J, Kouvetakis J and Menéndez J 2009 *Phys. Rev. Lett.* **102** 107403

[10] Mathews J, Beeler R T, Tolle J, Xu C, Roucka R, Kouvetakis J and Meneéndez J 2010 *Appl. Phys. Lett.* **97** 221912

[11] Chen R, Lin H, Huo Y, Hitzman C, Kamins T L and Harris J S 2011 *Appl. Phys. Lett.* **99** 181125

[12] Tseng H H, Wu K Y, Li H, Mashanov V, Cheng H H, Sun G and Soref R A 2013 *Appl. Phys. Lett.* **102** 182106

[13] Gupta J P, Bhargava N, Kim S, Adam T and Kolodzey J 2013 *Appl. Phys. Lett.* **102** 251117

[14] Sun G, Soref R A and Cheng H H 2010 *J. Appl. Phys.* **108** 033107

[15] D'Costa V, Cook C, Birdwell A, Littler C, Canonico M, Zollner S, Kouvetakis J and Menéndez J 2006 *Phys. Rev. B* **73** 125207

[16] Madelung O 2012 *Semiconductors: Data Handbook* (Berlin, Heidelberg: Springer)

[17] Adachi S 2009 *Properties of Semiconductor Alloys: Group-IV, III–V and II–VI Semiconductors* (Chichester, U.K.: Wiley) John Wiley & Sons, Wiley Online Laborary Online ISBN: 9780470744383

[18] Chuang S L 2008 *Physics of Photonic Devices*, 2nd edn. (John Wiley & Sons) ISBN: 978-O-470-29319-5

[19] Agrawal G P and Dutta N K 1986 *Long Wavelength Semiconductor Lasers* (New York: Van Nostrand Reinhold)

[20] Soref R and Larenzo J 1986 *IEEE J. Quantum Electron.* **22** 873

[21] Hilsum C 1974 *Electron. Lett.* **10** 259

[22] Sze S and Irvin J 1968 *Solid State Electron.* **11** 599

[23] Su S J, Wang W, Zhang G Z, Hu W X, Bai A Q, Xue C L, Zuo Y H, Cheng B W and Wang Q M 2011 *Acta Phys. Sin.* **60** 028101 (in Chinese)

[24] Haynes J R and Nilsson N G 1964 *Proceedings of VIIth International Conference on Physics of Semiconductors* (Paris: Dunod), p. 21

[25] Conradt R and Aengenheister J 1972 *Solid. State. Commun.* **10** 321